Research Article | Vol. 9, No. 9 | 1 Sep 2018 | BIOMEDICAL OPTICS EXPRESS 3983
Biomedical Optics EXPRESS

Comparative study on the detection of early dental caries using thermo-photonic lock-in imaging and optical coherence tomography

ELNAZ B. SHOKOUHI, MARJAN RAZANI, ASHISH GUPTA, AND NIMA TABATABAEI*

York University, Hybrid Biomedical Optics Lab, Department of Mechanical Engineering, 4700 Keele Street, Toronto, Ontario M3J 1P3, Canada
**Nima.Tabatabaei@lassonde.yorku.ca*

Abstract: Early detection of dental caries is known to be the key to the effectiveness of therapeutic and preventive approaches in dentistry. However, existing clinical detection techniques, such as radiographs, are not sufficiently sensitive to detect and monitor the progression of caries at early stages. As such, in recent years, several optics-based imaging modalities have been proposed for the early detection of caries. The majority of these techniques rely on the enhancement of light scattering in early carious lesions, while a few of them are based on the enhancement of light absorption at early caries sites. In this paper, we report on a systemic comparative study on the detection performances of optical coherence tomography (OCT) and thermophotonic lock-in imaging (TPLI) as representative early caries detection modalities based on light scattering and absorption, respectively. Through controlled demineralization studies on extracted human teeth and μCT validation experiments, several detection performance parameters of the two modalities such as detection threshold, sensitivity and specificity have been qualitatively analyzed and discussed. Our experiment results suggests that both modalities have sufficient sensitivity for the detection of well-developed early caries on occlusal and smooth surfaces; however, TPLI provides better sensitivity and detection threshold for detecting very early stages of caries formation, which is deemed to be critical for the effectiveness of therapeutic and preventive approaches in dentistry. Moreover, due to the more specific nature of the light absorption contrast mechanism over light scattering, TPLI exhibits better detection specificity, which results in less false positive readings and thus allows for the proper differentiation of early caries regions from the surrounding intact areas. The major shortcoming of TPLI is its inherent depth-integrated nature, prohibiting the production of depth-resolved/B-mode like images. The outcomes of this research justify the need for a light-absorption based imaging modality with the ability to produce tomographic and depth-resolved images, combining the key advantages of OCT and TPLI.

OCIS codes: (170.0170) Medical optics and biotechnology; (040.6808) Thermal (uncooled) IR detectors, arrays and imaging; (110.6820) Thermal imaging; (350.5340) Photothermal effects; (110.4500); Optical coherence tomography; (170.1850) Dentistry.

References and links

1. E. Kidd, *Essentials of Dental Caries the Disease and Its Management,* 3rd ed. (Oxford University Press, 2005).
2. *Dental Caries: The Disease and its Clinical Management,* 3rd ed. (Wiley-Blackwell, 2015).
3. M. Mohanraj, V. Prabhu, and R. Senthil, "Diagnostic methods for early detection of dental caries - A review," International Journal of Pedodontic Rehabilitation **1**, 29–36 (2016).
4. R. A. Bagramian, F. Garcia-Godoy, and A. R. Volpe, "The global increase in dental caries. A pending public health crisis," Am. J. Dent. **22**(1), 3–8 (2009).
5. J. D. Bader, D. A. Shugars, and A. J. Bonito, "A systematic review of the performance of methods for identifying carious lesions," J. Public Health Dent. **62**(4), 201–213 (2002).
6. M. S. Hopcraft and M. V. Morgan, "Comparison of radiographic and clinical diagnosis of approximal and occlusal dental caries in a young adult population," Community Dent. Oral Epidemiol. **33**(3), 212–218 (2005).

#327330 https://doi.org/10.1364/BOE.9.003983
Journal © 2018 Received 4 Apr 2018; revised 23 Jul 2018; accepted 26 Jul 2018; published 2 Aug 2018

Biomedical Optics EXPRESS

7. L. Karlsson, "Caries detection methods based on changes in optical properties between healthy and carious tissue," Int. J. Dent. **2010**, 270729 (2010).
8. M. J. S. C. White, Pharoah, *Oral Radiology: Principles and Interpretation,* 7th ed. (Elsevier Health Sciences, 2013).
9. A. P. Dhawan, B. D'Alessandro, and X. Fu, "Optical imaging modalities for biomedical applications," IEEE Rev. Biomed. Eng. **3**, 69–92 (2010).
10. Y.-S. Hsieh, Y.-C. Ho, S.-Y. Lee, C.-C. Chuang, J. C. Tsai, K.-F. Lin, and C.-W. Sun, "Dental optical coherence tomography," Sensors (Basel) **13**(7), 8928–8949 (2013).
11. N. Tabatabaei, A. Mandelis, and B. T. Amaechi, "Thermophotonic lock-in imaging of early demineralized and carious lesions in human teeth," J. Biomed. Opt. **16**, 071402 (2011).
12. M.-T. Tsai, H.-C. Lee, C.-K. Lee, C.-H. Yu, H.-M. Chen, C.-P. Chiang, C.-C. Chang, Y.-M. Wang, and C. C. Yang, "Effective indicators for diagnosis of oral cancer using optical coherence tomography," Opt. Express **16**(20), 15847–15862 (2008).
13. J. Espigares, A. Sadr, H. Hamba, Y. Shimada, M. Otsuki, J. Tagami, and Y. Sumi, "Assessment of natural enamel lesions with optical coherence tomography in comparison with microfocus x-ray computed tomography," J. Med. Imaging (Bellingham) **2**(1), 014001 (2015).
14. Y. Shimada, A. Sadr, M. F. Burrow, J. Tagami, N. Ozawa, and Y. Sumi, "Validation of swept-source optical coherence tomography (SS-OCT) for the diagnosis of occlusal caries," J. Dent. **38**(8), 655–665 (2010).
15. C. Sinescu, M. L. Negrutiu, C. Todea, C. Balabuc, L. Filip, R. Rominu, A. Bradu, M. Hughes, and A. G. Podoleanu, "Quality assessment of dental treatments using en-face optical coherence tomography," J. Biomed. Opt. **13**(5), 054065 (2008).
16. D. Fried, J. Xie, S. Shafi, J. D. Featherstone, T. M. Breunig, and C. Le, "Imaging caries lesions and lesion progression with polarization sensitive optical coherence tomography," J. Biomed. Opt. **7**(4), 618–627 (2002).
17. D. Fried, M. Staninec, C. L. Darling, K. H. Chan, and R. B. Pelzner, "Clinical Monitoring of Early Caries Lesions using Cross Polarization Optical Coherence Tomography," *Proceedings of SPIE–the International Society for Optical Engineering* **8566**(2013).
18. D. Fried, M. Staninec, C. Darling, H. Kang, and K. Chan, "Monitoring tooth demineralization using a cross polarization optical coherence tomographic system with an integrated MEMS scanner," *Proceedings of SPIE–the International Society for Optical Engineering* **8208**(2012).
19. J. C. Simon, H. Kang, M. Staninec, A. T. Jang, K. H. Chan, C. L. Darling, R. C. Lee, and D. Fried, "Near-IR and CP-OCT imaging of suspected occlusal caries lesions," Lasers Surg. Med. **49**(3), 215–224 (2017).
20. A. Baumgartner, S. Dichtl, C. K. Hitzenberger, H. Sattmann, B. Robl, A. Moritz, A. F. Fercher, and W. Sperr, "Polarization-sensitive optical coherence tomography of dental structures," Caries Res. **34**(1), 59–69 (2000).
21. J. Walther, J. Golde, L. Kirsten, F. Tetschke, F. Hempel, T. Rosenauer, C. Hannig, and E. Koch, "In vivo imaging of human oral hard and soft tissues by polarization-sensitive optical coherence tomography," J. Biomed. Opt. **22**(12), 1–17 (2017).
22. P. Ngaotheppitak, C. L. Darling, and D. Fried, "Measurement of the severity of natural smooth surface (interproximal) caries lesions with polarization sensitive optical coherence tomography," Lasers Surg. Med. **37**(1), 78–88 (2005).
23. J. Golde, F. Tetschke, J. Walther, T. Rosenauer, F. Hempel, C. Hannig, E. Koch, and L. Kirsten, "Detection of carious lesions utilizing depolarization imaging by polarization sensitive optical coherence tomography," J. Biomed. Opt. **23**(7), 1–8 (2018).
24. Y. Shimada, H. Nakagawa, A. Sadr, I. Wada, M. Nakajima, T. Nikaido, M. Otsuki, J. Tagami, and Y. Sumi, "Noninvasive cross-sectional imaging of proximal caries using swept-source optical coherence tomography (SS-OCT) in vivo," J. Biophotonics **7**(7), 506–513 (2014).
25. G. M. C. T. Astarita, *Infrared Thermography for Thermo-Fluid-Dynamics,* 1st ed. (Springer-Verlag Berlin Heidelberg, 2013).
26. W. W. O. Breitenstein and M. Langenkamp, *Lock-in Thermography: Basics and Use for Evaluating Electronic Devices and Materials,* 1st ed., Springer Series in Advanced Microelectronics (Springer-Verlag Berlin Heidelberg, 2003).
27. Y.-K. An, J. Min Kim, and H. Sohn, "Laser lock-in thermography for detection of surface-breaking fatigue cracks on uncoated steel structures," NDT Int. **65**, 54–63 (2014).
28. C. Meola, G. M. Carlomagno, A. Squillace, and A. Vitiello, "Non-destructive evaluation of aerospace materials with lock-in thermography," Eng. Fail. Anal. **13**(3), 380–388 (2006).
29. N. Tabatabaei, A. Mandelis, M. Dehghany, K. H. Michaelian, and B. T. Amaechi, "On the sensitivity of thermophotonic lock-in imaging and polarized Raman spectroscopy to early dental caries diagnosis," J. Biomed. Opt. **17**(2), 025002 (2012).
30. A. Ojaghi, A. Parkhimchyk, and N. Tabatabaei, "First step toward translation of thermophotonic lock-in imaging to dentistry as an early caries detection technology," J. Biomed. Opt. **21**(9), 096003 (2016).
31. M. Razani, A. Parkhimchyk, and N. Tabatabaei, "Lock-in thermography using a cellphone attachment infrared camera," AIP Adv. (in press).
32. M. Streza, B. Belean, I. Hodisan, and C. Prejmerean, "Improving lock-in thermography detection of microgaps located at the tooth-filling interface using a phase versus amplitude image signal extraction approach," Measurement **104**, 21–28 (2017).

Biomedical Optics EXPRESS

33. H. Schneider, K.-J. Park, M. Häfer, C. Rüger, G. Schmalz, F. Krause, J. Schmidt, D. Ziebolz, and R. Haak, "Dental applications of optical coherence tomography (OCT) in criology," Applied Sciences **7**(5), 472 (2017).
34. A. Aden, A. Anthony, C. Brigi, M. S. Merchant, H. Siraj, and P. H. Tomlins, "Dynamic measurement of the optical properties of bovine enamel demineralization models using four-dimensional optical coherence tomography," J. Biomed. Opt. **22**(7), 076020 (2017).
35. J. S. Holtzman, K. Osann, J. Pharar, K. Lee, Y. C. Ahn, T. Tucker, S. Sabet, Z. Chen, R. Gukasyan, and P. Wilder-Smith, "Ability of optical coherence tomography to detect caries beneath commonly used dental sealants," Lasers Surg. Med. **42**(8), 752–759 (2010).
36. Y. Shimada, H. Nakagawa, A. Sadr, I. Wada, M. Nakajima, T. Nikaido, M. Otsuki, J. Tagami, and Y. Sumi, "Noninvasive cross-sectional imaging of proximal caries using swept-source optical coherence tomography (SS-OCT) in vivo," J. Biophotonics **7**(7), 506–513 (2014).
37. S. Kaiplavil and A. Mandelis, "Truncated-correlation photothermal coherence tomography for deep subsurface analysis," Nat. Photonics **8**(8), 635–642 (2014).
38. D. C. Adler, S.-W. Huang, R. Huber, and J. G. Fujimoto, "Photothermal detection of gold nanoparticles using phase-sensitive optical coherence tomography," Opt. Express **16**(7), 4376–4393 (2008).

1. Introduction

Dental caries is a chronic infectious disease caused by the bacterial deposits in dental biofilms which produce acids when digesting the carbohydrates in foods. The production of acid causes the plaque pH to fall below 5, resulting in demineralization of hydroxyapatite crystals in the outermost layer of the tooth (i.e., enamel) [1]. However, the acid produced is constantly neutralized by saliva, increasing the pH and yielding remineralization [1, 2]. Over time, the demineralization and remineralization cycles occur periodically and when the net demineralization rate exceeds that of remineralization, early dental caries are formed [1, 2]. If the early caries is not treated, at this crucial early stage, the demineralization will continue and yield irreversible conditions such as advanced caries and cavities [1, 2]. Despite the promising therapeutic techniques offered by the state-of-the-art in preventive dentistry [3], dental caries continues to be a major public health challenge in both children and adults [4]. The reason behind this ineffectiveness is due to the fact that the success of therapeutic techniques in stopping the progression of dental caries to cavities, strongly rely on detection of caries at the very early stages of formation [3]. X-ray imaging and visual-tactile inspection are the conventional examination methods widely adapted in dental clinics for detection of different stages of dental caries. However, studies based on these methods often show an overall low sensitivity and high specificity which means that a large number of lesions may be missed, especially those at clinically challenging surfaces such as occlusal and proximal [5–7]. To address this shortcoming in detection sensitivity, recently, several optics-based caries detection methods have been developed. Unlike x-ray imaging modalities, which are carcinogenic and may cause molecular changes in biologic systems [8], optics-based technologies use non-ionizing laser light that is not only safe for tissue but also very sensitive to small changes in tissue properties [9]. Moreover, these systems are non-invasive as the generated temperature gradients are not strong enough to induce permanent damage in biological tissues [9]. The detection mechanism of majority of optics-based technologies rely on enhancement of light scattering in early carious lesion (e.g., optical coherent tomography or OCT [10]) while few of them operate based on enhancement of light absorption in early caries (e.g., thermophotonic lock-in imaging or TPLI [11]). In past two decades, researchers have made significant progress in development and validation of early caries detection modalities. Yet, minimal research effort has been focused on objective comparison of the basic capabilities of scattering-based and absorption-based contrast mechanisms such as detection specificity. As such, in this paper, we report on a systemic comparison of OCT and TPLI (as representative techniques based on light scattering and absorption, respectively), identifying the advantages and limitations of each technique in detecting artificially-induced/standardized early dental caries.

Optical coherence tomography is a promising non-invasive and non-contact optical imaging modality capable of providing 3-dimensional sub-surface morphology of biological tissue microstructure with micron-scale resolution [10]. In OCT, the distance between optical

Biomedical Optics EXPRESS

reflections from different layers of tissue is measured through interferometry by retrieving the time delay of the light reflected from optical interfaces (A-scan) through Fourier transformation. A series of A-scans along a line on sample surface creates cross-sectional or B-scan images, while scanning the sample surface in two dimensions provides volumetric data [10]. Owing to the ability of OCT in providing high-resolution 3-dimensional images, OCT has recently gained popularity in Dentistry research for diagnosis and screening of dental diseases and oral cancer [12–16]. Tsai *et al.* [12] showed that OCT provides high resolution pathological information for an effective diagnosis of oral cancer at its early stages and detection of oral squamous cell carcinoma. To assess various types of enamel lesions *in vivo*, a study by Espigares *et al.* [13] compared OCT with micro-focus x-ray computed tomography (μCT) images, concluding that OCT shows the lesions as areas of increased signal intensity and that OCT has great potential to be used in clinical practice for detection and screening of caries. In another study, Shimada *et al.* [14] used OCT for detection of the challenging clinical cases of occlusal caries and reported a superior sensitivity in detection of early caries on occlusal surfaces using OCT over the existing clinical modalities of x-ray imaging and visual/tactile inspection. Due to shallow imaging depth of the system (~1-2mm), however, other diagnostic imaging modalities have to be used for diagnosis of more advanced caries. While A- and B-scan OCT images were studied in these dental OCT works, Sinescu *et al.* [15] used *en-face* OCT images to examine the material defects of dental prostheses as well as micro-leakages at prosthetic interfaces. *En-face* OCT imaging appears to be an optimal option for delivering the complex tomographic information of OCT [15]. Another major advancement in the field has been the introduction of cross-polarization OCT (CP-OCT) by Fried *et al.* [16–19] for elimination of the obscuring effects of surface Fresnel reflections and thus more reliable quantification and monitoring of various stages of carious lesions. Polarization sensitive OCT (PS-OCT) has also been utilized for imaging composite restorations and mineralization defects [20–22]. The additional contrast channels offered by PS-OCT, such as depolarization and retardation [23], are believed to have better linkage to the mineralization status of dental hard tissues compared to the reflectivity profiles of conventional OCT. However, conventional OCT and CP-OCT are still mainstream in dental OCT research mostly due to the complexities associated with instrumentation and data processing of PS-OCT data as well as the additional instrumentation cost of PS-OCT. Despite the wealth of information provided by dental OCT studies, correlation of findings among studies has proven to be quite challenging, especially for detection of early dental caries. This is mostly due to two fundamental inconsistencies in the design of experiments: First, most studies report performance parameters (e.g., sensitivity, specificity, etc) by studying natural caries (i.e., unstandardized samples) which introduces a significant degree of variability in studied samples as optical properties of tooth and its susceptibility to demineralization are multifactorial phenomena, being function of parameters such as patient's oral health status, diet, ethnicity, etc. Second, most studies base the early caries detection criteria on the contrast obtained between the suspected early caries lesion and the healthy areas at its immediate proximity as opposed to a more global reference such as the contrast between suspected lesion and the healthy areas on the whole surface of the tooth. Due to these inconsistencies, variations in terms of sensitivity and specificity of OCT to early stages of caries formation are found in the literature with an overall observation of better sensitivity of OCT compared to radiography but no significant difference in specificity for early detection of caries at challenging surfaces such as proximal [24].

While OCT provides three dimensional map of light-reflecting interfaces in biological tissues such as micro pores introduced by demineralization in tooth, light absorption-based technologies such as thermophotonic lock-in imaging (TPLI) produce map of subsurface features absorbing the specific incident laser radiation (e.g., Calcium and phosphate as the byproducts of demineralization). TPLI is a non-destructive testing technology that performs diagnostic imaging using infrared cameras, therefore a thermography technique [25] Most of

Biomedical Optics EXPRESS

the applications of thermography are passive; for example, imaging of temperature differences in parts and structures (e.g., heat losses in buildings) or biological tissues (e.g., skin temperature mapping). In active thermography, on the other hand, an energy source (e.g., laser) is introduced to the system to produce a thermal contrast between the feature of interest and the background in a controlled manner [25]. That is, a modulated light source (e.g., laser) is utilized to induce heat periodically at a certain frequency while the local surface temperature modulation is captured by an infrared camera [26]. In this arrangement, presence of subsurface defects (e.g. early caries), alters the registered surface temperature profiles that the IR camera captures, thus creating a contrast between the intact and defective regions. One example of active thermography is lock-in thermography [25, 26], in which the altered surface temperature profiles are revealed through the lock-in demodulation signal processing algorithm. Lock-in thermography is a popular non-destructive testing technique which has predominantly been used in industry for interrogation of manufactured parts and industrial samples such as detection of fatigue cracks in structures [27] or defective aerospace component [28]. However, applications of lock-in thermography in Dentistry has also been recognized and investigated. Tabatabaei *et al.* [29] incorporated lock-in thermography for the first time for imaging of early stages of demineralization in dental tissues using a mid-wavelength infrared (MWIR) camera. The study established a long term strategy for detecting early dental caries and its diagnostic outperformance over other emerging technologies such as polarized Raman spectroscopy [29]. Ojaghi and Tabatabaei [30] demonstrated diagnostic imaging of early caries using low-cost and passively cooled long-wave infrared cameras (LWIR) [29, 30]. Our most recent work in this area demonstrates feasibility of detecting early dental caries using cellphone attachment infrared cameras which cost as low as ~$250, opening the door for commercialization and translation of the TPLI technology to Dentistry as an inexpensive end user product [31]. TPLI has also been utilized in Dentistry research for applications other than early caries detection. Streza *et al.* [32] performed a comparative study between lock-in thermography and optical microscopy to examine adhesion between dental fillings and the dental hard tissue. The outcome of the study demonstrated that lock-in thermography has superior photothermal contrast in the presence of micro-gaps and testing of dental interfaces where optical microscopy showed no defects at the enamel interface [32].

The above review of literature suggests that both OCT and TPLI have the promise of detecting caries at early stages of formation when preventive measures can be utilized to not only arrest the caries lesion but also heal it through remineralization therapeutic techniques. Sections below intend to explore and compare the advantages and limitations of TPLI and CP-OCT (as one of the mainstream OCT extension used in Dentistry research [33]) in detection of early stages of caries by studying standardized human samples containing artificially-induced caries.

2. Materials and methods

2.1 Thermophotonic lock-in imaging

Detailed explanation of the experimental setup, Fig. 1, and the theoretical foundation of TPLI can be found in our previous publications [11, 29, 30]. Briefly, in TPLI experimental setup, the excitation source consists of a fiber coupled (multimode; core diameter = 200 μm) continuous wave near-infrared laser (808nm; Jenoptik, Jena, Germany) which is regulated by a laser controller unit (Ostech, Berlin, Germany) in order to allow for modulation of laser intensity at 2Hz and to maintain an average optical intensity of 2 W/cm^2 on the sample surface. The 2Hz laser modulation frequency yields a theoretical resolution of 90μm in enamel. The distance between the optical fiber and the sample is adjusted to get a 15-mm diameter beam size on the interrogated surface of the sample. A frame grabber, a long-wave infrared (LWIR) camera (Gobi 640; Xenics, Leuven, Belgium), and a multifunctional data acquisition board (National Instruments, Austin, Texas, NI USB-6363 BNC) are used to

Biomedical Optics EXPRESS

capture and record the emitted thermal radiation from samples subjected to intensity modulated laser excitation.

The multifunctional data acquisition board synchronously generates three signals: reference pulse train, in-phase, and quadrature reference signals. The reference pulse train indicates the beginning of each modulation cycle for averaging purposes. The in-phase reference signal is responsible for modulating the intensity of the laser beam. As such, the in-phase reference signal is in-phase with the laser modulation while there is a 90° phase lead between the in-phase and quadrature reference signals. The LWIR camera is focused on the surface of the sample which is securely mounted on a LEGO block. During experiments, camera images are acquired at a maximum frame rate of 50 frames per second while at the same time the values of in-phase and quadrature signals are recorded. Subsequently, the acquired images are weighed and averaged using the instantaneous readings of the two reference signals to yield in-phase (S^0) and quadrate (S^{90}) images [30]. The amplitude and phase for each pixel are then calculated by applying Eq. (1), resulting in calculation of amplitude and phase images, respectively.

$$A = \sqrt{(S^0)^2 + (S^{90})^2} \quad and \quad \varphi = \arctan\left(\frac{S^{90}}{S^0}\right). \tag{1}$$

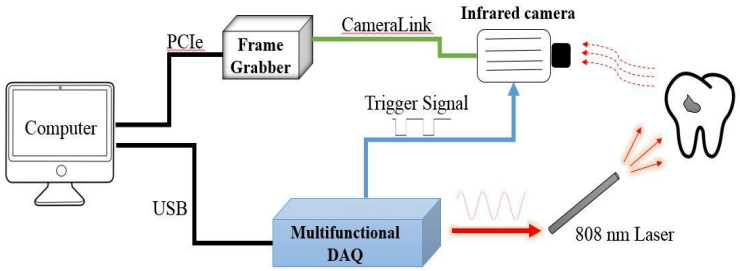

Fig. 1. Schematic representation of the developed thermophotonic lock-in imaging (TPLI) system.

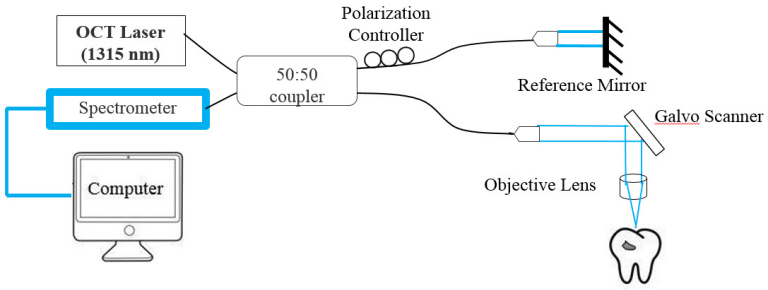

Fig. 2. Schematic representation of the developed spectral-domain optical coherence tomography (OCT) system. The polarization controller is adjusted to yield interference in the cross-polarization state.

2.2 Spectral domain optical coherence tomography

Figure 2 depicts a schematic of the developed spectral-domain OCT system. The light source is a near-infrared superluminescent diode (Exalos; Switzerland) emitting at 1315nm with a 115nm FWHM and a maximal output power of 30mW. After passing through a fiber coupler, the source light is coupled into a fiber-based Michelson interferometer. The splitting ratio of the 2 × 2 fiber coupler is 50/50. To minimize reflection signals from samples, a polarization controller is used in the reference arm to adjust polarization to the cross-polarization state.

Biomedical Optics EXPRESS

Subsequently, the interference spectrum is captured in the spectrometer by a line scan camera, composed of 2048 pixels, with a maximum scan/acquisition rate of 147 kHz. The theoretical axial resolution of the system is approximately 5 µm in tooth and the theoretical lateral resolution is 10 µm. Optical power at sample is ~7mW and the signal-to-noise (SNR) of the built OCT system is >100 dB. The developed data acquisition and processing program scans the OCT beam along the surface of the sample using the two galvo scanners (GS) and performs the inverse Fourier transform operation on the spectral-domain signals registered by the spectrometer, thus creating 3D tomographic images of subsurface reflectors (e.g., early caries). The amplitudes of the backscattered light in a form of B-scan (i.e., cross-sectional image) were used for studying the effects of demineralization. Moreover, following the convention in the field [15], integrated *en-face* images were produced by integrating the A-line values located 20 µm to 500µm below the enamel surface. Rejection of the superficial 20 µm enabled us to remove the obscuring effects of surface specular reflections from the signals more efficiently (see Appendix, Fig. 10).

2.3 Micro computed tomography

In this study, micro Computed Tomography (Skyscan 1272 high-resolution µCT system, Bruker MicroCT, Kontich, Belgium) with a camera pixel size of 7.4 µm was used as a gold standard for qualitative validation of OCT and TPLI experiments. After imaging with OCT and TPLI, tooth samples were placed in a cylindrical tube and positioned on the stage such that the treatment window would fall in the field of view of the detector. To minimize the effects of beam hardening, a 0.5-mm Al/Cu filter was used with scan rate of 100 kV and exposure time of 1251 ms per frame. NRecon software (NRecon, version 1.7.1.6., Skyscan, Kontich, Belgium) was used to perform reconstruction on the projections and DataViewer software was further used to display the captured cross-sectional slices on X, Y, and Z axis.

2.4 Dental sample collection and controlled demineralization protocol

Following the bio- and laser safety regulations at York University, anonymous extracted human teeth were collected from local oral surgeons. Samples were stored in tight container containing distilled water to maintain constant hydration and were kept in the laboratory fume hood at room temperature. The surfaces of the samples were not polished or altered in any way prior to the experiments. For controlled demineralization of dental samples, a lactic acid-based solution was prepared. The solution was an acidified gel (pH of 4.5), consisting of 0.1 M lactic acid and 0.1 M NaOH which is gelled with addition of 6% w/v hydroxyethylcellulose [11, 30]. This acidified gel is known to mimic the properties of bacterial plaques on enamel, providing an environment for cyclic occurrence of demineralization and remineralization and thus creation of early caries. As such, 4 teeth with no visible defect or white spot lesions were selected and cleaned namely samples 1 to 4 (Table 1). After drying in air, the surface of tooth was covered by transparent nail polish, leaving a small window of a specific surface area uncovered, namely the treatment window. Sample was then submerged upside down in a test tube containing 25 ml of acidic gel and left in the gel for various durations of the demineralization, Table 1 [11, 30]. After each treatment step/period, the sample was removed from the gel, cleaned under running water and dried in air [11, 30]. Then, the transparent nail polish was removed from the interrogated surface with acetone and the sample was again rinsed with tap water. Acid exposure time of treatment windows for samples 1 and 2 was 10 days in order to produce advanced early caries. Sample 3 was designed to have 3 treatment windows with acid exposure times of 2, 4 and 8 days in left, middle and right windows, respectively. Imaging studies (sequence: OCT, TPLI then µCT) were carried out on samples 1-3 after completion of the abovementioned demineralization schedule. To study systems' performance parameters as a function of demineralization time, the treatment window of sample 4 was incrementally demineralized. Imaging studies (OCT followed by TPLI) were conducted after each demineralization step.

Biomedical Optics EXPRESS

The treatment window's cumulative acid exposure duration at each imaging study session is depicted in Table 1. The μCT experiment was conducted on sample 4 after the final demineralization step (i.e., 15 days).

In preparation for OCT and TPLI imaging, the samples were air-blown and dried for 10 seconds to simulate the condition under which the inspection of caries is typically carried out in clinical scenarios. Additionally, to monitor the appearance of the demineralization window in each demineralization interval, a high magnification CCD camera was used to take photographs of the sample. Once imaged with the OCT and TPLI systems, the same procedure was repeated to apply additional demineralization in the treatment window.

Table 1. Samples' demineralization schedule and schematic of imaging study sequence.

Photograph	Study Target	Total Demineralization Period(s) Applied to Treatment Window
sample 1 	Detection of Advanced Early Caries on Smooth Surface	10 days
sample 2 	Detection of Advanced Early Caries on Occlusal Surface	10 days
sample 3 	Detection Threshold	Left window: 2days Middle Window: 4days Right Window: 8Days
sample 4 	Detection Sensitivity	1day →2days→ 3days→ 4days→ 5days→ 6days→ 7days→ 8days→ 10days→ 15days
Sequence of Imaging Modalities Used at Each Demineralization Step: OCT ➡ TPLI ➡ μCT		

2.5 Data processing and analysis

To conduct a comparison of the images captured from OCT and TPLI at various stages of demineralization, the thermophotonic phase images at 2Hz and integrated *en-face* images derived from OCT were normalized. This was done to account for the small day-to-day changes in the experimental setup (e.g., laser source power) and tooth. For TPLI phase images, normalization was carried out by applying Eq. (2). That is, in any given phase image, the average pixel value of an intact reference area was subtracted from each pixel value.

$$\text{Normalized image pixel value} = \text{pixel value} - \text{average phase value of healthy region} \quad (2)$$

For integrated *en-face* OCT images, a similar normalization was performed:

$$\text{Normalized image pixel value} = \frac{\text{pixel value}}{\text{average amplitude value of healthy region}} \quad (3)$$

In order to quantify the diagnostic performances of the two systems, the following statistical analysis was conducted on the longitudinal demineralization study of the sample exposed to the demineralizing gel for various durations. First, the field of view of OCT and TPLI experiments were matched, followed by calculation of mean and standard deviation of contrast within the treatment window in each image. Then, the contrast value of each pixel in a given image was statistically compared to the mean and standard deviation of the treatment window within the same image with 95% confidence. Following this analysis, pixels having significantly different contrast compared to that of the treatment window were identified as true negative and false negative if they were located outside and inside the treatment window, respectively. Similarly, pixels showing no significantly different contrast compared to that of the treatment window were identified as false positive and true positive if they were located

Biomedical Optics EXPRESS

outside and inside the treatment window, respectively. Following these quantifications, sensitivity and specificity values were calculated and the corresponding receiver operating characteristic (ROC) curves were produced.

3. Results and discussion

3.1 Detection of advanced early caries

To examine the performances of OCT and TPLI in detecting advanced stages of early caries, teeth samples which were demineralized for 10 days on the smooth (sample 1) and occlusal (sample 2) surfaces were imaged. The visual photographs of these samples were acquired after drying with compressed air, Fig. 3(a) and 3(b); rectangles depict the location of treatment windows. The photographs indicate the presence of white spot lesions on both samples, suggesting presence of early caries that have progressed well into the enamel layer (i.e., advanced early caries). In the OCT B-scan and integrated *en-face* images of the samples (Fig. 3(c)-(f)), the presence of the advanced enamel caries is well-recognized with a sharp contrast as a result of enhancement of light scattering within the treated region. Consequently, the demineralized regions appear bright in both B-mode and *en-face* images. This observation is consistent with reports of other researchers [34, 35]. Moreover, the B-mode/cross sectional image of Fig. 3(c) suggests that the enhancement in light scattering within the superficial caries region has been to an extent that the light photons could not effectively probe the underlying dental-enamel-junction (DEJ). For the healthy areas surrounding the treatment region, however, the light backscattering is not significant enough to mask the underlying structures as the tooth surface was protected against the demineralizing acid by the nail polish coating. As a result, DEJ can clearly be recognized in the untreated areas in the cross-sectional image of the smooth surface caries, Fig. 3(c). The B-mode OCT image of the advanced occlusal caries, Fig. 3(d), is also showing enhanced light scattering within the treated region. However, the DEJ cannot be resolved in this image due to the large thickness of enamel in the occlusal region and the limited imaging depth of OCT. Similar to OCT, the presence of lesions is clearly observed in the TPLI phase image taken at 2Hz after 10 days of demineralization, Figs. 3(g)-(h). Selective absorption of laser light at caries sites results in shifting of the centroid of the thermal-wave field and causes a phase shift in the thermal signals registered from caries areas compared to those collected from intact regions. The increase in light absorption at caries sites occurs as a result of absorption of laser light by the by-products of demineralization. Light absorption is further enhanced by the local enhancement of light scattering at caries as it results in increase in the local laser light flux within the caries area.

Compared to images taken with OCT, TPLI images offer a much larger field of view of the tooth with similar detection sensitivity. Another key difference between the performances of OCT and TPLI in detecting dental caries is the detection specificity (i.e., ability to yield minimal false positives). Figures 3(d) and 3(f) suggest that although the treated area appears with an enhanced contrast in the image, there are other areas outside the treatment windows which also show up as bright in both B-mode and integrated *en-face* images, yellow arrows in Figs. 3(d) and 3(f). Figures 3(i) and 3(j) show the μCT slices taken from the bright areas inside and outside the treatment window, respectively, along the dashed lines indicated in Fig. 3(f). These μCT slices clearly show the presence of early caries in the treatment window but no indication of mineral loss outside the treatment window and in the area where the OCT *en-face* image displays enhancement in contrast (yellow arrows). The characteristic mineral profile of early caries (i.e., area of mineral loss close to surface, protected by a thin healthy layer) is clearly resolved in the μCT slice taken from the treated area which speaks to the effectiveness of the artificial demineralization protocol adhered to in this study. As such, our results suggest that while the integrated *en-face* and B-scan OCT images indicate ability of OCT in detecting advanced stages of smooth surface and occlusal early caries as areas of enhanced light scattering, structural non-homogeneities other than those caused by

Biomedical Optics EXPRESS

demineralization induce a similar effect in OCT images; thus, creating false positive readings. Presence of false positives speaks to the non-specific nature of light scattering contrast mechanism which is enhanced as a result of discontinuities in refractive index, not necessarily caused by demineralization. While non-specific nature of OCT images of early caries has also been reported by other investigators [14, 36], recent studies suggest that this problem can be alleviated using PS-OCT [21]. TPLI images, on the other hand, display enhancement of contrast only within the treated area because laser excitation is selectively absorbed in these regions; thus, yielding minimal false positive readings. The downside of TPLI imaging, however, is that these images are governed by the physics of heat diffusion and as such are depth integrated rather than depth resolved and cannot provide tomographic maps of samples or create transverse/B-mode type images resolving internal tissue features. In summary, qualitative analysis of results of Fig. 3 suggest that both optical systems have sufficient detection sensitivity to detect advanced stages of early caries on smooth and occlusal surfaces; however, detection specificity is better in TPLI imaging.

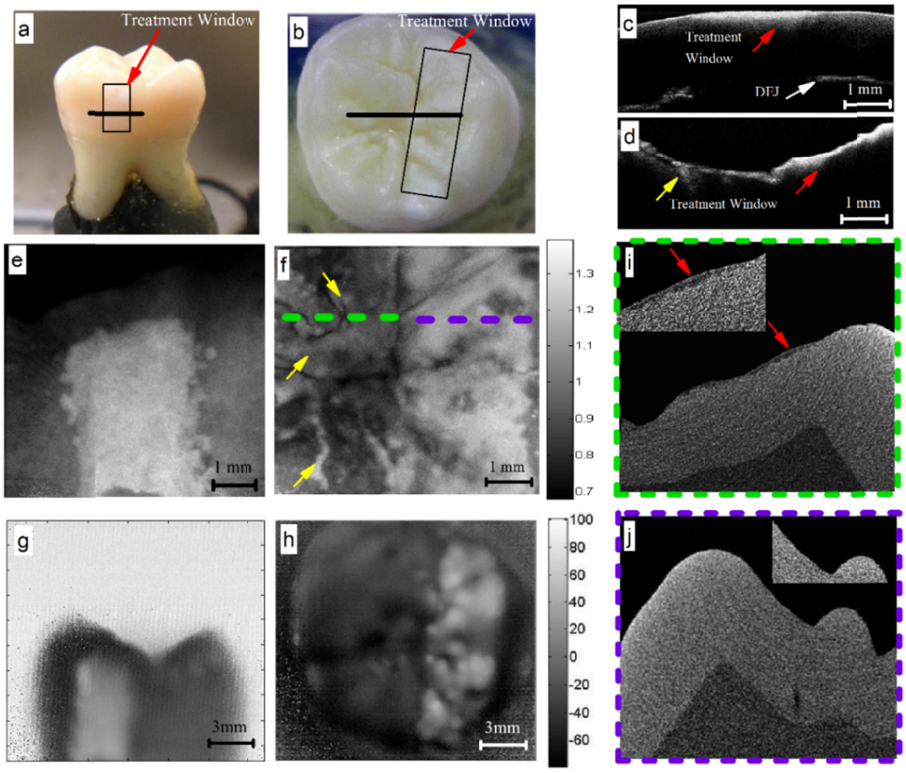

Fig. 3. Photographs of simulated advanced caries on (a) smooth and (b) occlusal surfaces; rectangles depict the location of treatment windows. Representative OCT B-mode images of (c) smooth surface and (d) occlusal caries samples along the solid lines indicated in panels (a) and (b), respectively. Integrated en-face OCT images at 10 days of treatment of (e) smooth and (f) occlusal caries samples. TPLI phase images obtained at 2-Hz modulation frequency at 10 days of treatment for (g) smooth surface (h) occlusal caries samples. (i) and (j) represent the µCT slices along the green and blue dashed lines in panel (f), respectively. Red and yellow arrows point to treatment window and false positives, respectively.

3.2 Detection threshold

In the context of detecting early dental caries, detection threshold is the smallest amount of demineralization that a diagnostic system can reliably detect. To study this performance parameter, a healthy tooth sample (sample 3) with three artificially-induced caries for 2, 4 and 8 days on the same surface was chosen (Fig. 4(a)).

Biomedical Optics EXPRESS

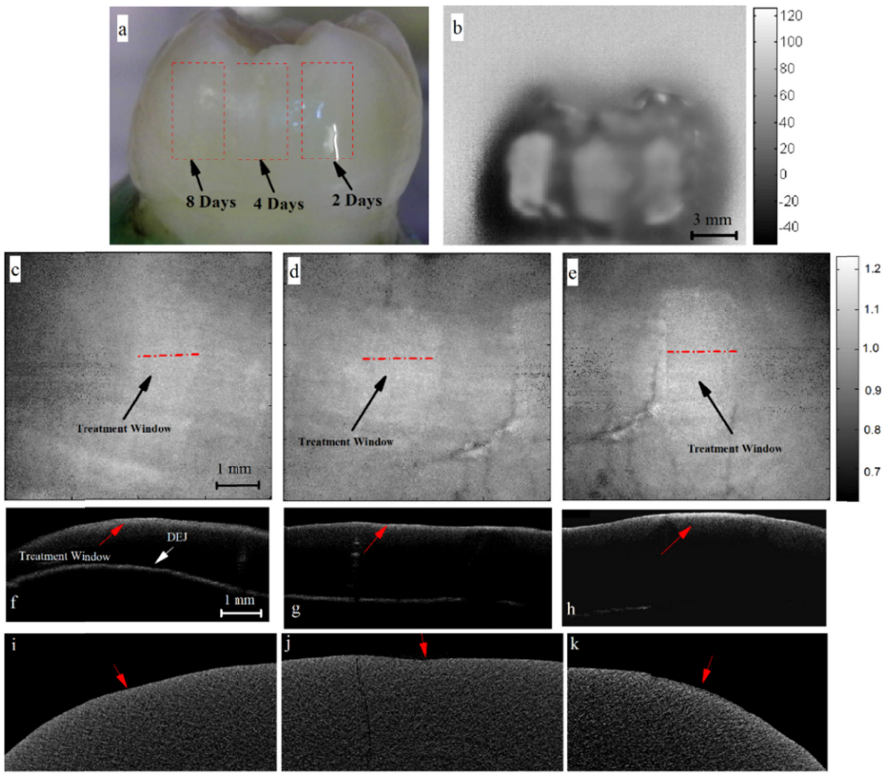

Fig. 4. (a) Visual image of tooth with artificially-induced caries at 3 locations. (b) TPLI phase image at 2-Hz modulation frequency. Integrated en-face OCT images at (c) 2 days, (d) 4 days, and (e) 8 days of demineralization. B-scan OCT images at (f) 2 days, (g) 4 days, and (h) 8 days of demineralization. µCT images at (i) 2 days, (j) 4 days, and (k) 8 days of demineralization.

As it can be seen in integrated *en-face* OCT images (Fig. 4(c)-(e)), the presence of demineralization is not visually detectable in 2- and 4-day treated windows due to the reflections with same level of contrast as of the treated regions originating from the healthy regions (i.e., false positives). However, the 8-day treated window shows a relatively higher contrast making it somewhat distinguishable, Fig. 4(e). Similar trend is observed in the OCT B-mode images (Fig. 4(f)-(h)): After 8 days of treatment, the demineralization has made further progress with reduced contrast at the DEJ as a result of overlaying demineralization; however, for 2- and 4-day windows, the DEJ appears with normal contrast due to the minimal enhancement of light scattering at demineralized areas. TPLI (Fig. 4(b)), on the other hand, is capable of detecting all the artificially-induced caries as higher contrast areas. The contrast of demineralized regions of 2 and 4 days are approximately equal but their contrast, compared to the intact areas of the enamel, are higher. The contrast at 8 days of demineralization shows a significant increase by visual inspection compared to other treatment windows as well as intact areas. The µCT images, panels (i)-(k), show vague indications of demineralization at 4 and 8 days of treatment.

Quantitative analysis was also conducted on images of Fig. 4. The bar plots of integrated *en-face* OCT images (Fig. 5(a)) along with their standard deviations indicate that OCT is statistically not specific enough to differentiate between healthy and each of the demineralized windows as the average integrated intensity values of all the treatment windows are within the standard deviation of the average integrated intensity value obtained from the untreated healthy region. However, the TPLI bar plots (Fig. 5(b)) suggest reliable increase of average normalized phase values between treated and healthy areas. The carious lesion formed as early as 2-days of demineralization can be differentiated due to an increase

Biomedical Optics EXPRESS

in average phase value above the range of standard deviation of phase value derived from the healthy region. The enhancement in detection threshold of TPLI over OCT is because of its basis on light absorption, thus effectively eliminating the background signals from healthy areas. Quantification of µCT images, panel (c), indicates that none of the treated windows can be reliably identified.

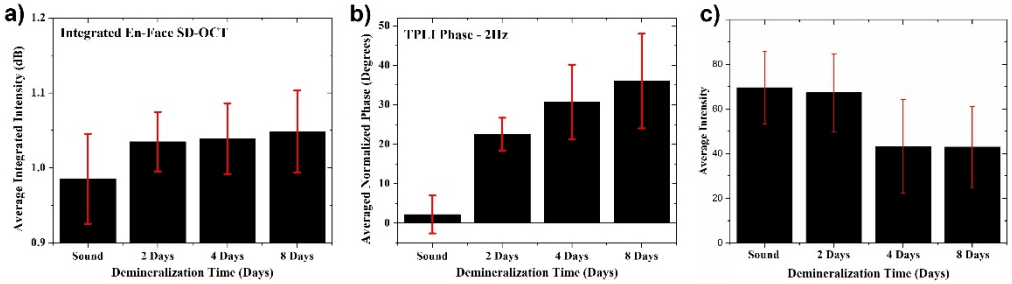

Fig. 5. Average contrast values from early caries and the associated standard deviation of mean for (a) optical coherence tomography (OCT) and (b) thermophotonic lock-in imaging (TPLI) and (c) µCT.

3.3 Detection sensitivity of OCT and TPLI

In the context of detection of early dental caries, detection sensitivity is linked to the ability of the diagnostic system in creating a noticeable change in contrast given an incremental increase in demineralization [35]. For this performance metric, a time-dependent demineralization procedure was followed on smooth surface of a relatively healthy tooth (sample 4) in small intervals of 1 day up to 8 days of demineralization and larger intervals up to 15 days of demineralization. Figures 6(a) and 6(b) show the photograph of the sample before and after application of 15-days of demineralization, respectively. In integrated *en-face* and B-scan OCT images (Figs. 6(c)-(n)), a very small change in contrast at the treatment window starts from day 1 of demineralization. This change in contrast gradually increases while reaching its maximum contrast at day 15 of demineralization. The presence of false positives (shown with yellow arrows) can be seen in many of these OCT images. Similar trend can be seen in TPLI phase images (Fig. 7) with contrast becoming reliably detectable at day 2 of demineralization, with gradual enhancement up to day 15 of demineralization. Thinning of enamel at the cervical margin (yellow arrow) results in underlying cementum acting as thermal impedance; thus, creating a change in contrast.

To further study the changes in average phase and integrated intensity values over various stages of demineralization progression, Fig. 8 shows the bars plots generated from OCT and TPLI images of Figs. 6 and 7. In integrated *en-face* OCT bar plots (Fig. 8(a)), it can be seen that with progression of artificially-induced early caries, there is a gradual enhancement in average integrated intensities. However, these small enhancements cannot be reliably realized due to the large standard deviations associated with the averaged contrast values. Consequently, it can be concluded that, in these experiments, OCT could not reliably differentiate between healthy and early carious lesions up to day 10 of treatment, setting the earliest reliable detection at 15 days of treatment. Figure 8(b) depicts the bar plots of the TPLI experiments. It can be seen that the detection threshold of TPLI can be distinguished as early as day 2 of demineralization. Moreover, a sizable change in contrast is observed as demineralization increases from 1 day of treatment to 15 days of treatment. The enhanced detection sensitivity of TPLI over OCT can be verified by calculating the amount of change in contrast at the detection threshold. For OCT, a 17.5% increase in contrast (1.011dB to 1.188dB) is observed after 15 days of treatment while TPLI contrast increases by 203% (–11.2° to 11.5°) only after 2 days of treatment. The TPLI enhancement in contrast at OCT detection threshold (i.e., 15 days of treatment) is found to be 424% (–11.2° to 36.3°). Panel

Biomedical Optics EXPRESS

(c) indicates the ability of µCT in detecting the well-developed early caries after 15 days of demineralization.

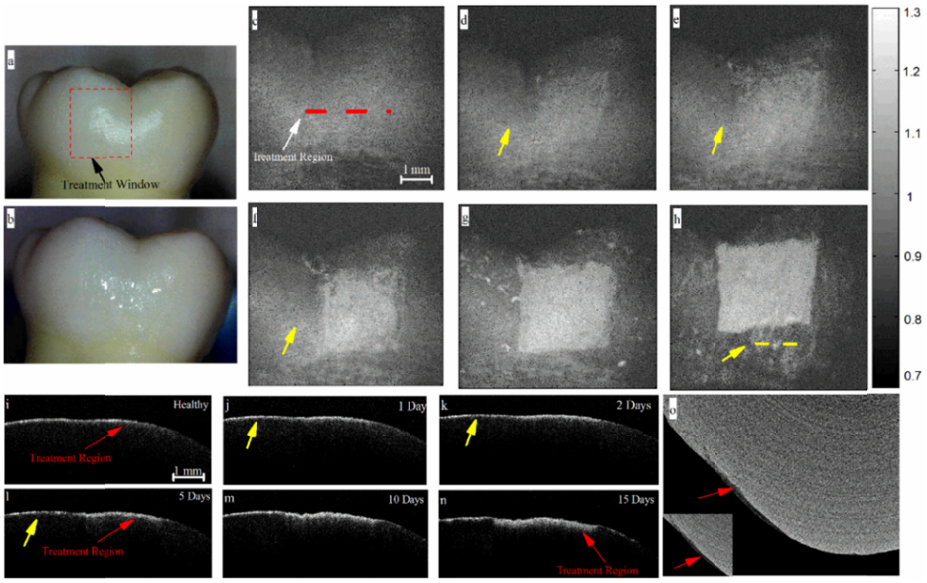

Fig. 6. Optical image of the smooth surface of extracted human molar (a) before demineralization and (b) after 15 days of demineralization on the treatment window. Integrated en-face OCT images at (c) 0 days, (d) 1 day, (e) 2 days, (f) 5 days, (g) 10 days, and (h) 15 days of demineralization. B-scan OCT images at (i) 0 days, (j) 1 day, (k) 2 days, (l) 5 days, (m) 10 days, and (n) 15 days of demineralization. (o) µCT image of 15-day treated sample.

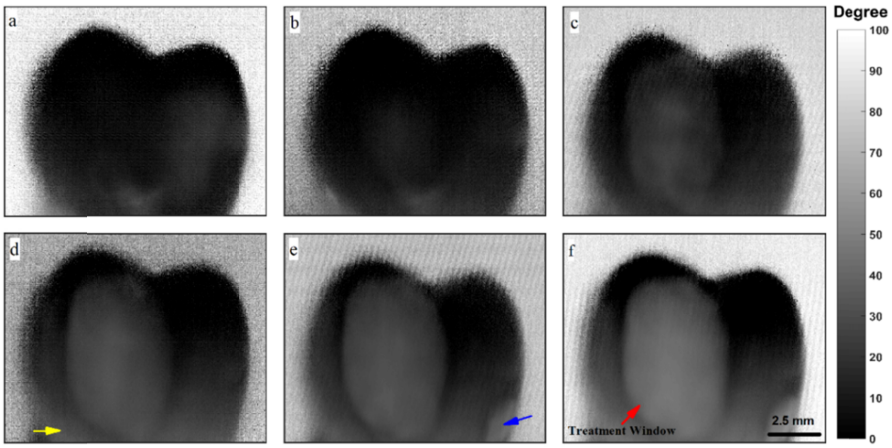

Fig. 7. TPLI phase images at 2-Hz modulation frequency at (a) 0 days, (b) 1 day, (c) 2 days, (d) 5 days, (e) 10 days, and (d) 15 days of demineralization. Yellow arrow points to change in contrast at cervical margin due to thinning of enamel and photothermal effects of the underlying cementum. Blue arrow points to part of the enamel which was damaged on day 10 of demineralization due to improper handling.

Figure 9 depicts results of the statistical analysis carried out using the procedure explained in the "data processing and analysis" section. Panels (a) and (b) highlight pixels statistically identified as demineralized (i.e., yellow pixels) by CP-OCT and TPLI, respectively, at different stages of demineralization. It can be seen that false positives (i.e., yellow pixels outside the treatment window) are significantly reduced in TPLI at 2 days (or more) of demineralization while such false positives are dominantly present in CP-OCT images up to 7

Biomedical Optics EXPRESS

or 8 days of demineralization. The tabulated sensitivity and specificity data in panel (c) confirms this visual observation. Finally, the ROC plot in panel (d) clearly show that both technologies are sensitive to detection of early caries. However, accumulation of TPLI data points in the upper left corner of the ROC plot confirms the more specific nature of TPLI over CP-OCT, especially at early stages of caries formation.

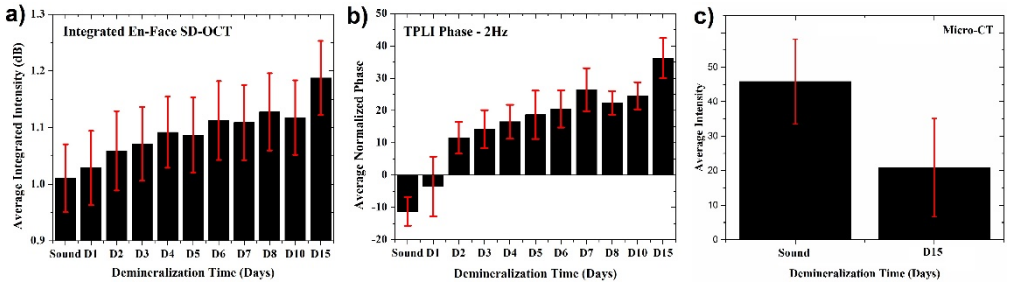

Fig. 8. Average contrast values from early caries and the associated standard deviation for (a) spectral-domain optical coherence tomography (OCT), (b) thermophotonic lock-in imaging (TPLI) and (c) µCT.

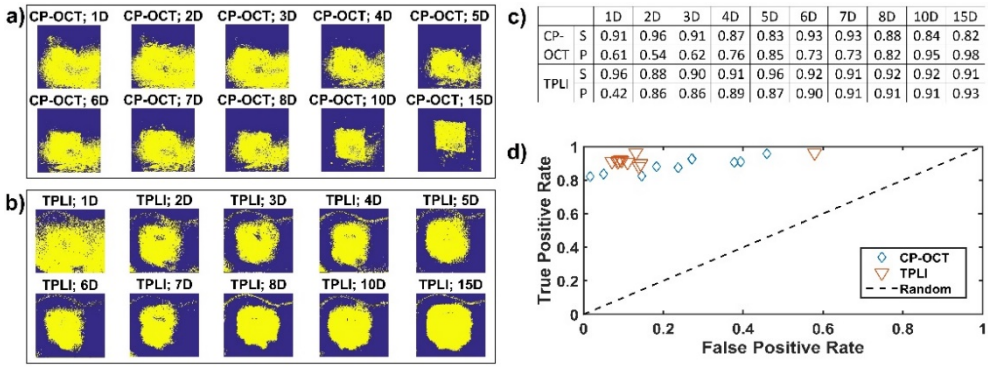

		1D	2D	3D	4D	5D	6D	7D	8D	10D	15D
CP-OCT	S	0.91	0.96	0.91	0.87	0.83	0.93	0.93	0.88	0.84	0.82
	P	0.61	0.54	0.62	0.76	0.85	0.73	0.73	0.82	0.95	0.98
TPLI	S	0.96	0.88	0.90	0.91	0.96	0.92	0.91	0.92	0.92	0.91
	P	0.42	0.86	0.86	0.89	0.87	0.90	0.91	0.91	0.91	0.93

Fig. 9. Statistically (CI: 95%) identified healthy (blue pixels) and demineralized (yellow pixels) at various stages of demineralization by (a) CP-OCT and (b) TPLI. Corresponding (c) sensitivity (S) and specificity (P) values and (d) receiver operating characteristic curve.

4. Summary

In this paper, we present results of a comparative study between cross-polarization spectral-domain optical coherence tomography (CP-OCT) and thermophotonic lock-in imaging (TPLI) in detecting early dental caries. The effectiveness of the adhered artificial demineralization protocol has been demonstrated through µCT validation experiments. Our experimental results suggests that both modalities have sufficient sensitivity for detection of well-developed early caries on occlusal and smooth surfaces; however, TPLI provides better sensitivity and detection threshold in detecting very early stages of caries formation which is deemed to be critical for effectiveness of therapeutic and preventive approaches in Dentistry. Moreover, due to the more specific nature of light absorption contrast mechanism over light scattering, TPLI exhibits better detection specificity which results in significantly less false positive readings and thus allows for proper differentiation of early caries regions from the surrounding intact areas. Other advantages of TPLI over OCT include larger field of view and less complexity of instrumentation. Major advantage of OCT over TPLI is its depth-selective and 3D tomographic nature over the intrinsic depth-integrated and 2D nature of TPLI which enables visualization of lesions within the 1-2 millimeter inspection range of OCT. 3D visualization of lesions enables quantification of parameters such as lesion depth and volume. Consequently, a light-absorption based imaging modality with the ability to produce

Biomedical Optics EXPRESS

tomographic and depth-resolved images is highly desired in the field of Dentistry as such modality would simultaneously offer the major advantages of OCT and TPLI. Truncated-correlation photothermal coherence tomography [37] and photothermal optical coherence tomography [38] are extensions of TPLI and OCT, respectively, which can theoretically provide such 3D maps based on absorption of light. Another interesting future work would be to examine the detection performances of TPLI and CP-OCT among deferent age groups as all samples studied in this manuscript were collected from adults.

Appendix

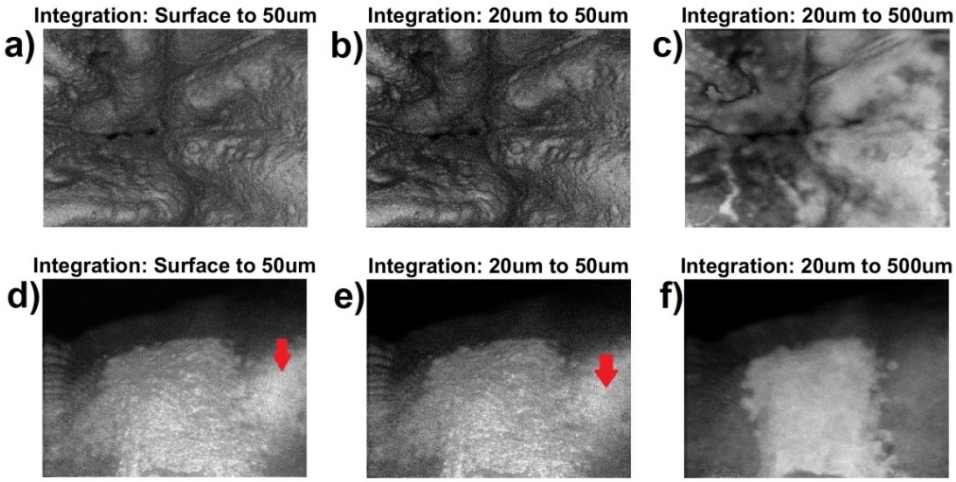

Fig. 10. Integrated CP-OCT *en-face* images using different integration limits along the depth, suggesting that inclusion of information from surface and superficial layers shallower than 50μm results in suboptimal contrast between early caries and surrounding healthy enamel as well as creation of false positive readings (arrows).

Funding

Natural Sciences and Engineering Research Council of Canada (RGPIN-2015-03666); Canadian Institutes of Health Research (DAN381313).

Acknowledgments

We are thankful to Dr. Martin Villiger (Harvard Medical School) and Professor Garrett Melenka (York University) for their invaluable technical assistance in experimentation. N.T. is grateful to the Natural Sciences and Engineering Research Council of Canada for the award of Discovery Grant, to the Canadian Institutes of Health Research for the award of Collaborative Health Research Projects grant, and to the Lassonde School of Engineering and the York University for their financial support.

Disclosures

The authors declare that there are no conflicts of interest related to this article.